
Univerzita Komenského v Bratislave

Fakulta matematiky, fyziky a informatiky



**Martin Žemlička**


**Autoreferát dizertačnej práce**

(Physical processes in disordered superconductors)

**na získanie akademického titulu philosophiae doctor**

**v odbore doktorandského štúdia:**
11-22-9 Fyzika kondenzovaných látok a akustika

**Bratislava, 30. 4. 2016**

**Dizertačná práca bola vypracovaná**
(v dennej forme doktorandského štúdia)

**na** katedre experimentálnej fyziky

**Predkladateľ:** Martin Žemlička
Fakulta matematiky, fyziky a informatiky
Univerzity Komenského
Mlynská dolina F1
842 48 Bratislava

**Školiteľ:** Miroslav Grajcar
Fakulta matematiky, fyziky a informatiky
Univerzity Komenského
Mlynská dolina F1
842 48 Bratislava

11-22-9 Fyzika kondenzovaných látok a akustika

**Predseda odborovej komisie:**

.....
Prof. RNDr. Peter Kúš, DrSc.
Fakulta matematiky, fyziky a informatiky
Univerzity Komenského
Mlynská dolina F1
842 48 Bratislava

In the dissertation we analyse the experimental results and their analysis obtained in our research. The summarization of the results is describe in third chapter of the thesis. Firstly we describe the optimisation of MoC thin film deposition, which produced films with high sheet resistance and critical temperature. We study transport properties of thin films with different thicknesses, which give us a better understanding of the behavior of our samples near the SIT. We show that the transition has fermionic scenario and corroborate this statement by STM measurements showing that the ratio between superconducting energy gap and critical temperature does not depend on the film thickness, while nonelastic scattering rapidly increases as thicknesses decreases below 10 nm. We focus on 3 nm MoC thin films on silicon and sapphire substrates, which are still in superconducting state, but very close to the SIT. Transport measurements in magnetic field imply, that there is significant electron-electron interaction described by Altshuler-Aronov theory. In the end, we will show the results of terahertz spectroscopy of our samples and analyze them with the same model as in the microwave experiment. We discuss the possible nonequilibrium superconducting effects, which should be reflected in our experiments as well as in the experiments performed by other groups on the thin films of similar materials.

## 0.1 Tuning the MoC deposition process

As mentioned earlier, the appropriate samples for our purposes are thin films close to the superconducting-insulator transition. In practice, they are ones which are still in superconducting state, but with a sheet resistance as high as possible. By tuning and analyzing the magnetron deposition process, we calibrate the procedure in order to obtain reproducible samples with well defined appropriate parameters.

### 0.1.1 Magnetron discharge analysis

In section **??** we generally described the reactive magnetron sputtering process. Our first inspiration came from [34], where the SIT on MoC thin films was observed at thickness of 13 Å. For the best deposition conditions we need to be in stable power regime. The sputtering power is defined by the current and voltage of the magnetron plasma discharge at specific pressure in the vacuum chamber. In order

to define best input parameters we measured the IV characteristics of the discharge at fixed argon pressure and different acetylene pressures (see 1).

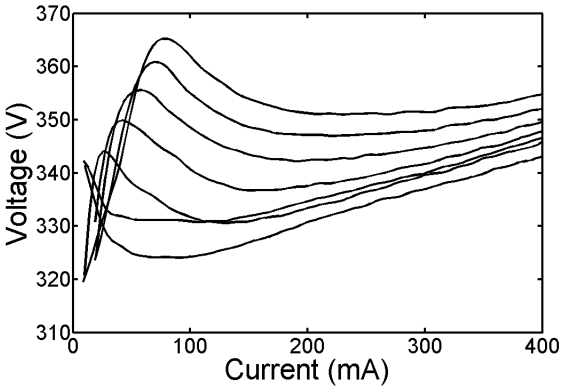


**Figure 1:** IV characteristics of the magnetron plasma discharge for different content of acetylene - the flow-controller opened to 0, 10, 20, 30, 40 and 50% from bottom to top

The stable regime occurs, when the IV characteristic reaches its local minimum (The changes of the discharge power are negligible for small current or voltage fluctuations). We decided to set the magnetron input current to 200mA, which is the most stable when the acetylene flow-controller is opened to 40% and corresponds to the voltage of 340 V.

### 0.1.2 Carbon content influence

The carbon content is tuned by the acetylene partial pressure. It defines the stoichiometry and the atomic structure of the resulting MoC thin film. In order to find the best deposition conditions for desired films we needed to prepare several series of films for different proportions of acetylene in the working gas keeping film thickness constant.

Film thickness was estimated from the sputtering rate calibration. In order to define it, we sputtered a testing thin film on silicon substrate with a lift-off lithography structure (see Fig. 2a) for exactly 3 minutes. After chemical etching the structure was measured by atomic force microscope (AFM) to get the information about the film thickness. Fig. 2b shows that the resulting film thickness was 30 nm, which implies a sputtering rate 10 nm / min.

Besides information on the film thickness, AFM provides us with the topography of the film surface, showing the roughness to be below 1.5 nm (see 2c). These results are promising towards the use of the thin films for patterning of the CPW res-

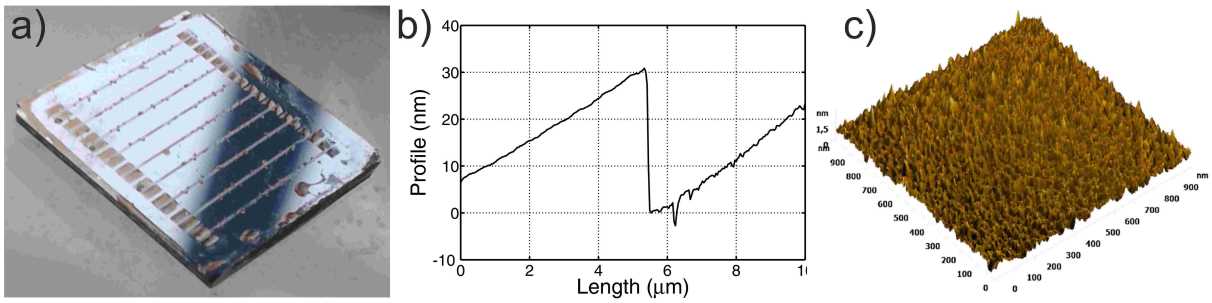


**Figure 2:** a) A silicon substrate for the lift-off lithography, b) AFM measurement of height profile, c) AFM topography

onator with embedded nanostructures. The roughness measurement was confirmed by X-ray reflectivity (XRR) for different film thicknesses (See the section below 0.2).

Since the sputtering rate was calibrated, we prepared several 10 nm thin films at different acetylene partial pressure and measured their RT-characteristics. The sheet resistance $R_{\square}$ and critical temperature $T_c$ were evaluated as a function of the acetylene pressure. The results can be seen in Fig. 3.

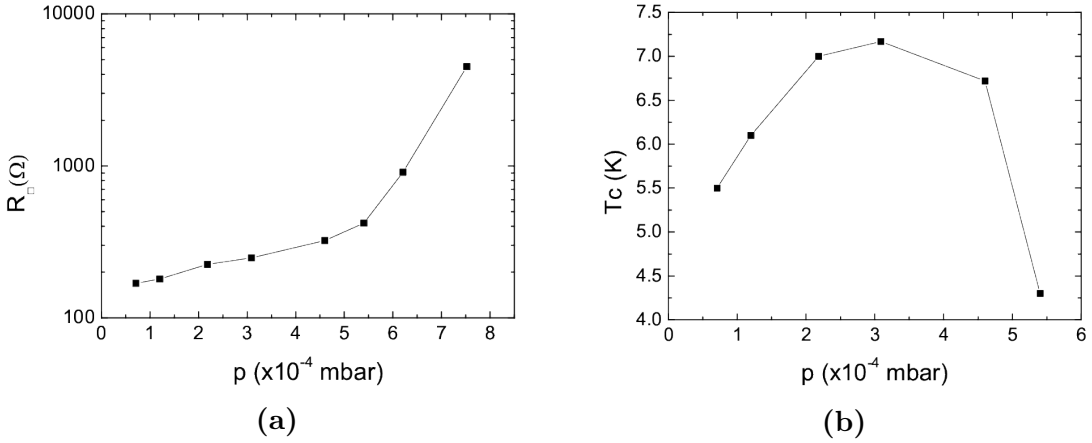


**Figure 3:** Acetylene partial pressure (carbon content) dependence of the sheet resistance (a) and critical temperature (b)

In order to maximize $T_c$, the optimal acetylene pressure is $3.0 \times 10^{-4}$ mbar, which corresponds to the acetylene flow-controller opened at 40%. Thin films produced above of $5.4 \times 10^{-4}$ mbar were not superconducting, limiting the sheet resistance for 10 nm superconducting film to 420 Ω.

Under the same conditions, we prepared a 30 nm thick sample set for X-ray diffraction measurement, from which we determined the atomic and crystallographic structure. The results are shown in Fig. 4.

The bottom curve corresponds to a pure molybdenum film deposited in argon atmosphere without acetylene. From bottom to top, the content of acetylene

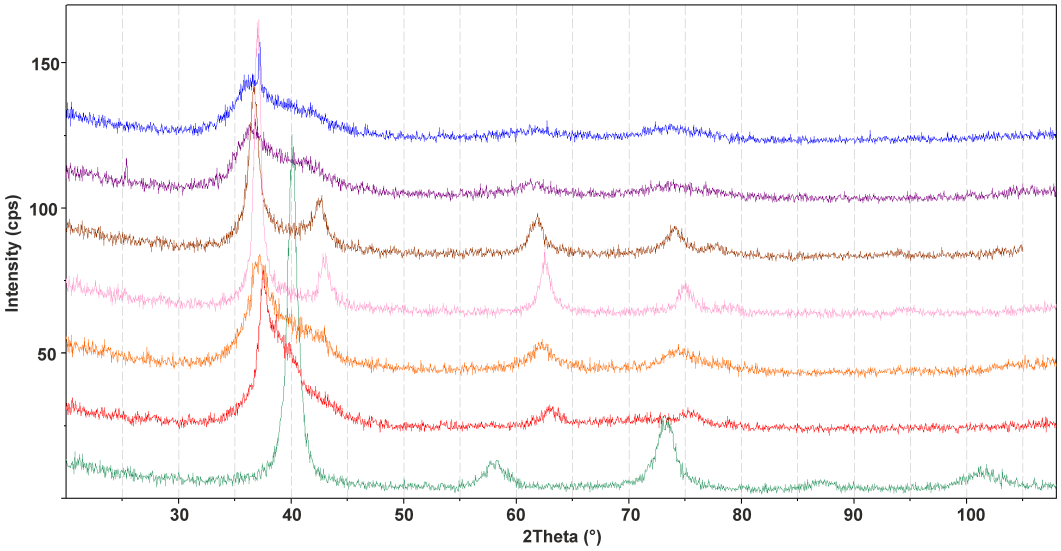


**Figure 4:** XRD measurements of samples prepared with different acetylene content - flow controller opened to 0, 10, 20, 30, 40, 50 and 60% from bottom to top

increases and the top curve represents a film prepared with the acetylene flow controller opened to 60 %. According to comparison with the XRD image database the relative positions of the peaks are associated with cubic crystallographic structure ($\delta$-phase). The peaks with the largest amount of carbon are significantly smeared, which implies that the major part of the film surface is amorphous. The optimal $T_c$ was achieved for acetylene content corresponding to 40%-opened flow controller (brown curve in Fig. 4). From absolute values of the peak positions, we determined the atomic lattice constant $a = 4.2$ Å. According to the database, the lattice constant for MoC with pure stoichiometry 1:1 is expected to be $a = 4.273$ Å. In detailed study in Ref. [66] it is explained that the change in carbon concentration from MoC to $MoC_{0.75}$ leads to a decrease of volume of the elementary atomic unit by 5%, corresponding to 1.7% decrease of the lattice constant. This completely agrees with our deviation of 0.07 nm.

We used VESTA 3D visualization program for structural models to obtain image of the MoC cubic structure. In Fig. 5, we compare the simulated cubic structure with a surface image obtained by STM topography measurement. The results clearly agree with the view of the structure in plane 111.

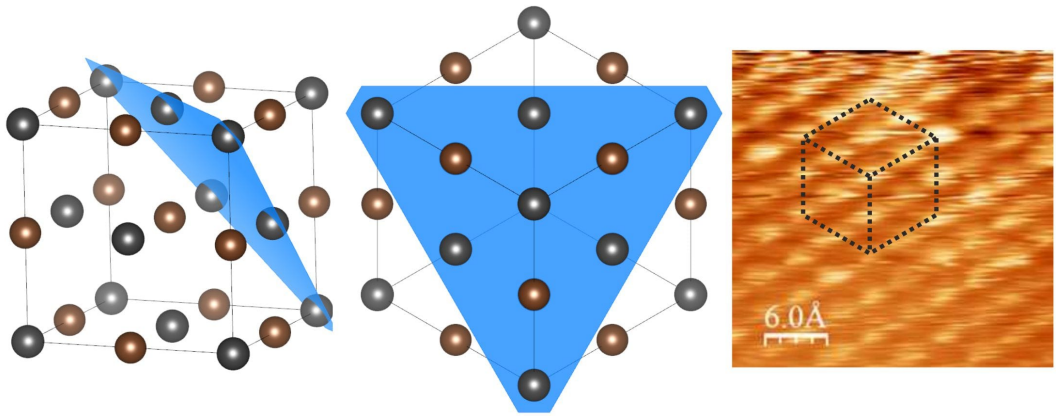


**Figure 5:** a),b) cubic structure obtained by simulation in VESTA software, c) STM topography in atomary level demonstrating the cubic phase on 111 plane

Since the STM is not precisely calibrated to define the exact values of length, the lattice constant couldn't be precisely measured. However, the qualitative surface image of the atomic structure in conjunction with the XRD results gives us sufficient evidence that the crystallographic phase of our sample is of cubic (NaCl like) type.

The stoichiometry was also analyzed by energy dispersive X-ray (EDX) method. This method requires a much thicker sample, so we prepared one 1000 nm film. The results of the measurement are shown in Fig. 6.

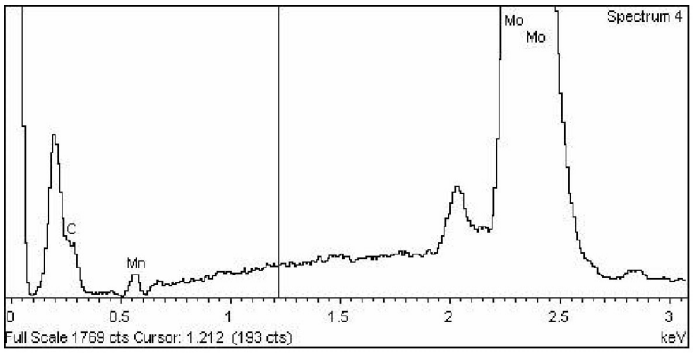


| Element | Weight% | Atomic% |
|---|---|---|
| C K | 17.68 | 62.81 |
| Mn K | 0.01 | 0.01 |
| Mo L | 83.58 | 37.17 |
| Totals | 101.27 | |

**Figure 6:** EDX measurement and corresponding table showing the content of individual elements in 1 $\mu$m MoC thin film

The atomic ratio of carbon and molybdenum is approximately 60:40 in this case. The increased proportion of carbon is possibly caused by amorphous carbon islands among crystalline grains of MoC.

More details about MoC thin film deposition and the optimization of deposition parameters are described in the publication [P2].

## 0.2 Transport properties

After the MoC thin films deposition was optimized, we decided to characterize the transport properties of prepared samples. Firstly, we measured the RT characteristics for samples of different thickness. From the results, we established the correlation between superconducting properties of the sample and the level of disorder, which gave us more detailed insight into phase transition between the superconducting and insulating state. Then we performed transport measurements in perpendicular direct magnetic field, from which we determined basic parameters such as upper critical field $B_{C2}$, superconducting coherence length $\xi_0$, diffusion coefficient $D$, Hall coefficient $R_H$, concentration of charge carriers $n$ or Ioffe-Regel disorder parameter $k_f l$.

### Thickness dependence

In order to verify whether the thickness estimation used in sample deposition corresponds to reality, we prepared four samples with thicknesses 5, 10, 15 and 20 nm and measured them using X-ray reflectivity (XRR) method, to obtain a the mass density and intensity profile, from which we can extract information about film thickness, density and roughness (see table 1).

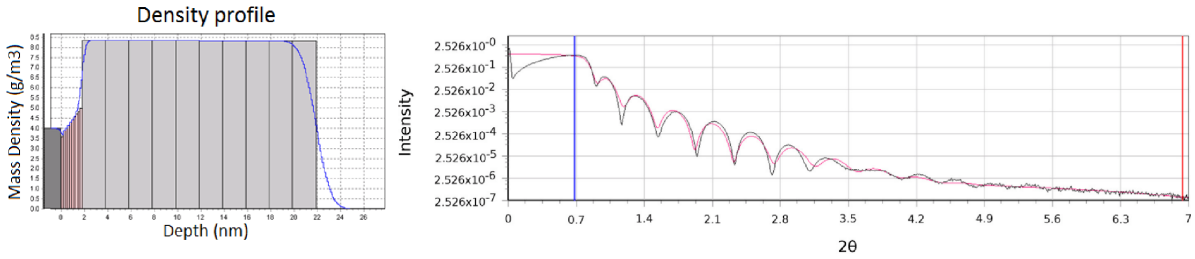


**Figure 7:** Density and intensity profile measured by XRR

The measured film thickness is in very good agreement with our prediction from the calibrated sputtering rate. The roughness measurement is consistent with AFM data (see Fig. 2) and the fact it is below 1.5 nm allows us to prepare structures with measurable kinetic inductance.

In transport experiments, we first measured the temperature dependence of sheet resistance for different thicknesses without an applied magnetic field. The results are shown in Fig. 8a.

The superconducting transitions are very sharp and it can be seen that with

| Sample | | 20nm | 15nm | 10nm | 5nm |
|---|---|---|---|---|---|
| thickness | [nm] | 20.08 | 13.67 | 11.20 | 4.74 |
| density | [g/cm$^3$] | 8.35 | 8.02 | 7.71 | 8.83 |
| roughness | [nm] | 1.00 | 0.78 | 1.25 | 1.26 |

**Table 1:** Results of X-ray reflectivity measurement (XRR) for various thickness MoC films.

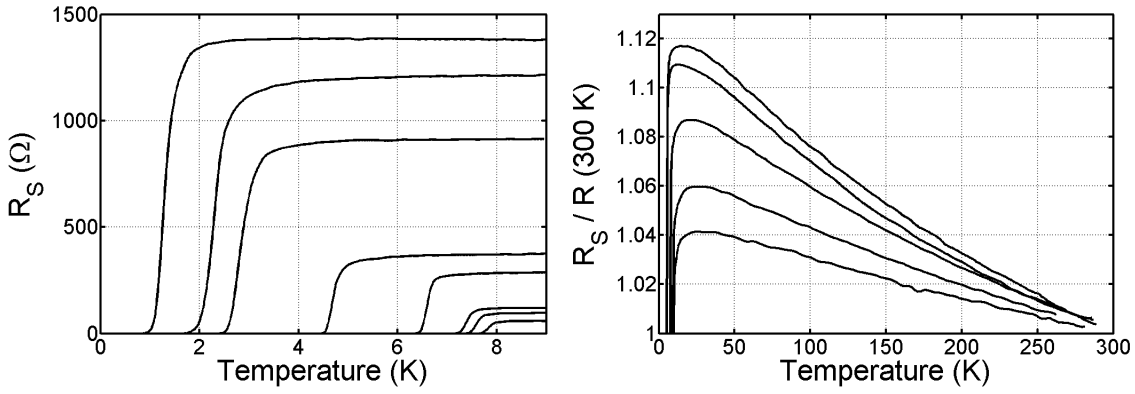


**(a)** **(b)**

**Figure 8:** RT characteristics for samples with thicknesses a) 30, 20, 15, 10, 10, 5, 5, 3 nm (from bottom to top) in zoomed window 0-8 K, b) 15, 10, 10, 5, 5 nm (from bottom to top) with temperature ranging from room temperature to superconducting transition

decreasing thickness, $R_\square$ increases and $T_c$ decreases. This behavior is characteristic for homogeneously disordered superconductors, in contrast with granular superconductors, where $T_c$ keeps its bulk value and the transition are broadened significantly. In total, we measured 8 samples with thicknesses ranging from 3 nm to 30 nm. There are two 10 nm and two 5 nm samples showing different $R_\square$ and $T_c$, which is caused by small changes in argon and acetylene pressures during the deposition process. We can therefore conclude that $R_\square$ correlates with superconducting transition onset better than film thickness.

The negative derivative $dR_\square/dT$ presented for all samples (fig. 8b) strongly indicates quantum corrections [33] to Drude conductivity caused by enhanced electron-electron interaction. From the measured data, we extracted the thickness dependence of $R_\square$ and $T_c$. The theoretical variation of $R_\square$ is predicted by classical percolation theory with the assumption that the thickness is proportional to the areal occupation probability in the percolation problem [34]. The thickness proportion of sheet resistance from this prediction is $R_\square(t) \sim (t - t_c)^{-1.3}$, where $t_c$ is minimum thickness for electrical continuity. From the fitting procedure (see fig. 9a) we determined the value $t_c = 1.3\ nm$.

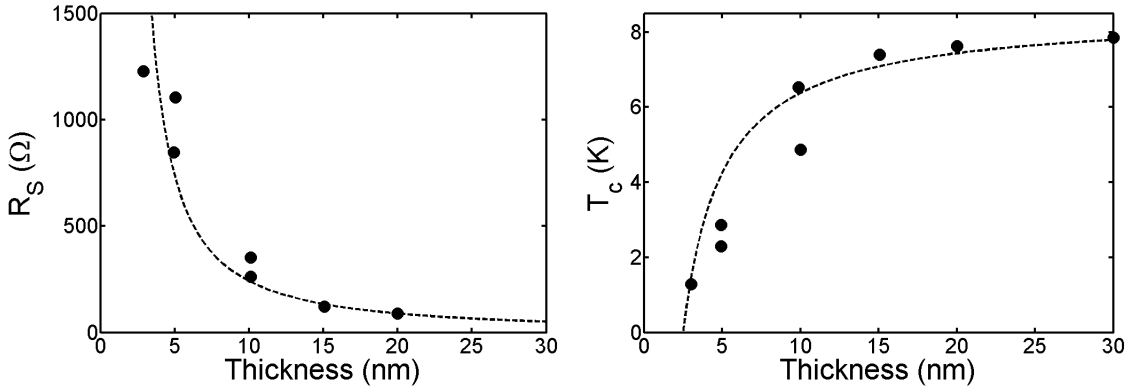


**Figure 9:** Thickness dependence of a) sheet resistance (dots) fitted with $R_{\square}(t) \sim (t - t_c)^{-1.3}$ (dashed line), b) critical temperature (dots) fitted with $T_c(t) = T_{c0}(1 - t_c/t)$ (dashed line)

The thickness dependence of $T_c$ (see fig. 9b) shows a strong decrease for thicknesses below 15 nm, which is close to double value of the coherence length $\xi(0) \approx 5.5\ nm$ determined from the upper critical field, as obtained from the magnetotransport measurements. It determines the range of superconducting attraction so the decrease of $T_c$ is caused by surface effects. As a theoretical approach, one can take the calculations made by Simonin [63], which considers the decrease in density of states because of the surface term in GL free energy. The thickness dependence of critical temperature is then expressed as:

$$T_c(t) = T_{c0}(1 - t_c/t), \tag{1}$$

where $T_{c0}$ is the bulk critical temperature and $t_c$ is the critical thickness where the superconductivity is destroyed. From the fit (Fig. 9b), we determined the parameters $T_{c0} = 8.5\ K$ and $t_c = 2.5\ nm$.

The resulting values of minimum thickness for electrical continuity and the superconducting critical thickness found in Ref. [34] are bit smaller: 0.4 nm and 1.3 nm respectively.

Enhanced electron-electron interactions imply the fermionic model of SIT, which means that the transition from superconductor to insulator state goes through the metallic state. This model, which describes the dependence of $T_c$ on $R_{\square}$ was developed by Finkelstein [61] as:

$$\log\left(\frac{T_c}{T_{c0}}\right) = \gamma + \frac{1}{\sqrt{2r}} \log\left(\frac{1/\gamma + r/4 - \sqrt{r}/2}{1/\gamma + r/4 + \sqrt{r}/2}\right), \tag{2}$$

where $r = R_{\square}e^2/(2\pi^2\hbar)$ is dimensionless resistance and $\gamma$ is the fitting parameter, which defines the ratio of the smaller value out of either the diffusive energy $\varepsilon/\tau$ ($\tau$ is the relaxation time in the normal state) or Thouless energy $\pi^2\hbar D/t^2$ ($D$ is the diffusion coefficient) to the non-renormalized condensation energy $k_B T_{c0}$, where $T_{c0} = 8.5$ K. The equation was used to fit the experimental data and the results are shown in Fig. 10

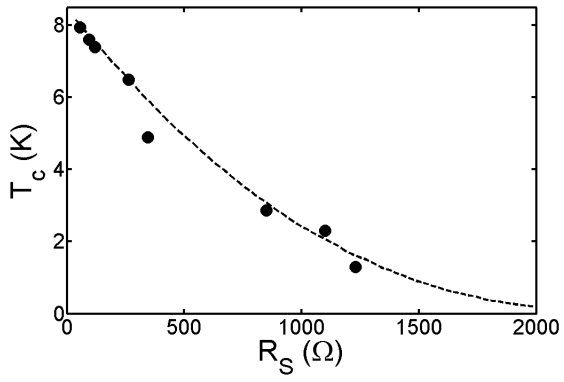


**Figure 10:** Critical temperature dependence on sheet resistance (dots) fitted with Finkelstein formula (dashed line)

The best fit was achieved for $\gamma = 8.3$ and $T_{c0} = 8.5\ K$. Similar result with $\gamma = 8.2$ was obtained in the original paper by Finkelstein for MoGe thin films with $T_{c0} = 7.2$ K.

The RT characteristic across the whole temperature range can be used to determine of the electron transport dimensionality. Standard Bloch–Grüneisen theorem describing the resistivity temperature dependence gives the positive temperature coefficient $dR_{\square}/dT > 0$. The sign is changed if the quantum corrections ascribed to weak localization and electron-electron interactions (Altshuler-Aronov) are significant. The correction to the conductivity depends on sample dimensionality and follows the relationship:

$$\Delta G^{WL} + \Delta G^{AA} = \begin{cases} A\sqrt{T} + BT^{p/2} & \text{for 3D} \\ G_{00} A_1 \log(k_B T\tau/\hbar) & \text{for 2D} \end{cases} \tag{3}$$

where $p \in (3/2, 2)$, $G_{00} = e^2/(2\pi^2/hbar)$ and $A, B, A_1$ are the normalization constants. We compared these predictions with the data measured on the MoC sample with 5 nm thickness in superconducting state as well as in normal state achieved by an applied magnetic field of 8 T (above $B_{c2}$). On the presented graph (see Fig. 11) we can see that the curves overlap above 20 K and follow the 3D power

law. Under this temperature, the superconducting fluctuations start to play a role and the curves differ. The superconducting conductance starts to increase and diverges to infinity at $T_c = 2.3\ K$, while the normal state conductance decreases logarithmically as in the 2D case.

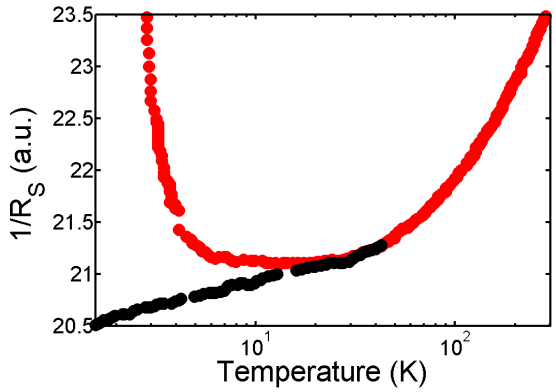


**Figure 11:** Temperature dependence of conductance for 5 nm MoC sample measured at 500 mK and magnetic field B=0 T (red dots) and B=8 T (black dots)

Finkelstein's mechanism becomes relevant, when the samples effectively behave as 2D. This condition seems to be satisfied in our case for all samples at low temperatures, but the strength of the $T_c$ suppression is given by the value of the constant $\gamma$. In order to analyze its value obtained from the fitting procedure, we performed magnetotransport and Hall-effect measurements.

### Magnetotransport and Hall measurements

From the RT characteristic measurement at different applied magnetic fields, one can estimate the temperature dependence of the upper critical magnetic field $B_{c2}(T)$. We performed such measurements and the results are shown in Fig. 12.

We can estimate the value of the upper critical field at zero temperature by Werthamer-Helfand-Hohenberg theory [67] and then the superconducting coherence length and diffusion coefficient can be determined by using the relations:

$$B_{c2}(0) = 0.69 \frac{dB_{c2}}{dT} T_c \tag{4}$$

$$\xi(0) = \sqrt{\frac{\phi_0}{2\pi B_{c2}(0)}} \tag{5}$$

$$D = 0.407 \frac{\pi k_B}{e} \left( \frac{dB_{c2}}{dT} \right)^{-1} \tag{6}$$

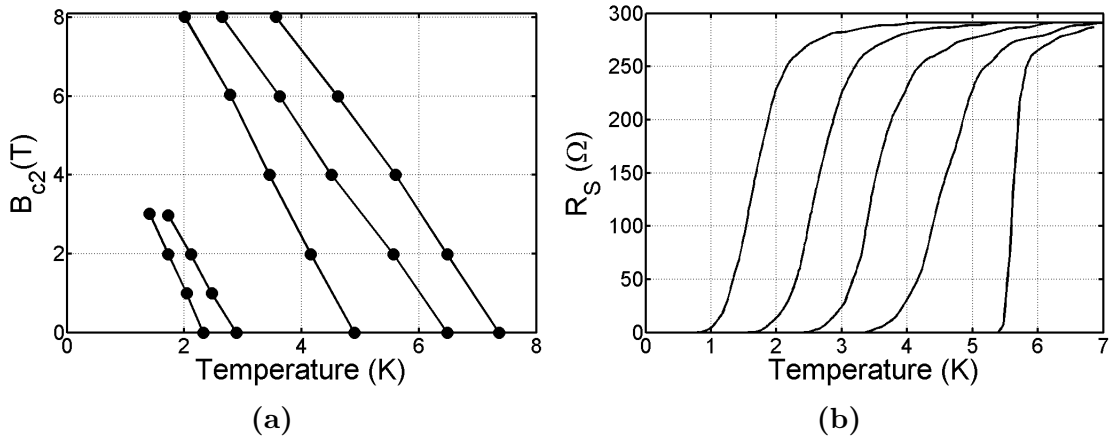


**Figure 12:** a) Temperature dependence of upper critical magnetic field for samples with thicknesses 5, 5, 10, 10 and 15 nm (from left to right), b) RT characteristics of 10 nm MoC sample measured at magnetic fields 0 -8 T (from right to left)

The results are summarized in Tab. 2. The calculated Thouless energy is not much bigger that the condensation energy $kT_c$, which is consistent with the fact, that the samples only behave as 2D at low temperatures. In this regime, when $\hbar/\tau \gg \pi^2\hbar D/d^2$, the suppression of $T_c$ given by Finkelstein's relation is very slight, which is inconsistent with our measurements. Since the same argument is also valid for MoGe [61, 68] and TiN [69–71] thin films, an alternative way to describe $T_c$ suppression with increasing disorder has to be found.

Additionally we performed Hall-effect measurements at 200 K in fields ranging from -8 to 8 T. From the results we determined the Hall coefficient $R_H$ and charge carrier densities $n = -1/eR_H$ for all samples, which are summarized in Tab. 2. It is surprising that the carrier density is almost constant at the value 1.7 $\times$ $10^{23}$ cm$^{-3}$, which is in contrast with the measurements on TiN thin films [71]. Therefore, the decrease of the thickness decreases mobility of quasiparticles in our samples.

| $t$ [nm] | $R_\square$ [Ω] | $T_c$ [K] | $R_H \times 10^{11}$ [ΩmT$^{-1}$] | $n \times 10^{23}$ [cm$^{-3}$] | $k_f l$ $k_f l$ | $B_{c2}$ [T] | $\xi$ [nm] | $D$ [cm$^2$/s] | $\pi^2\hbar D/d^2$ [K] |
|---|---|---|---|---|---|---|---|---|---|
| 30 | 56 | 7.95 | - | - | - | - | - | - | |
| 20 | 95 | 7.6 | - | - | - | - | - | - | |
| 15 | 120 | 7.4 | 3.75 | 1.7 | 4.1 | 10.7 | 5.48 | 0.52 | 17.4 |
| 10 | 263 | 6.5 | 3.75 | 1.7 | 2.8 | 9.4 | 5.78 | 0.53 | 40 |
| 10 | 344 | 4.9 | 3.13 | 1.9 | 2 | 9.5 | 5.8 | 0.39 | 29.4 |
| 5 | 850 | 2.86 | 3.8 | 1.7 | 1.46 | 5.3 | 7.8 | 0.39 | 118 |
| 5 | 1100 | 2.3 | 3.8 | 1.7 | 1.34 | 5.3 | 7.8 | 0.33 | 100 |
| 3 | 1227 | 1.3 | 3.9 | 1.7 | 1.3 | - | - | - | - |

**Table 2:** Basic parameters of MoC samples with different thicknesses, obtained and calculated from results determined by magneto-transport measurements

The level of disorder can be quantified by the Ioffe-Regel parameter $k_f l$, where $k_f$ is the Fermi wave number and $l$ is the mean free path. The quantum phase transition is expected at $k_f l \approx 1$. From our measurements, we can estimate $k f_l$ in the free electron model as follows:

$$k_f l = \frac{\hbar (3\pi^2)^{2/3}}{e^{5/3}} \left[ \frac{R_H^{1/3}}{R_\square d} \right] \tag{7}$$

In Fig. 13 we show the dependence of critical temperature $T_c$ and sheet conductance $1/R_\square$ on this parameter. From linear extrapolation, we can see that the conductance reaches zero if $k_f l$ equals unity, which is in agreement with Ioffe-Regel criterion for phase transition to insulating state.

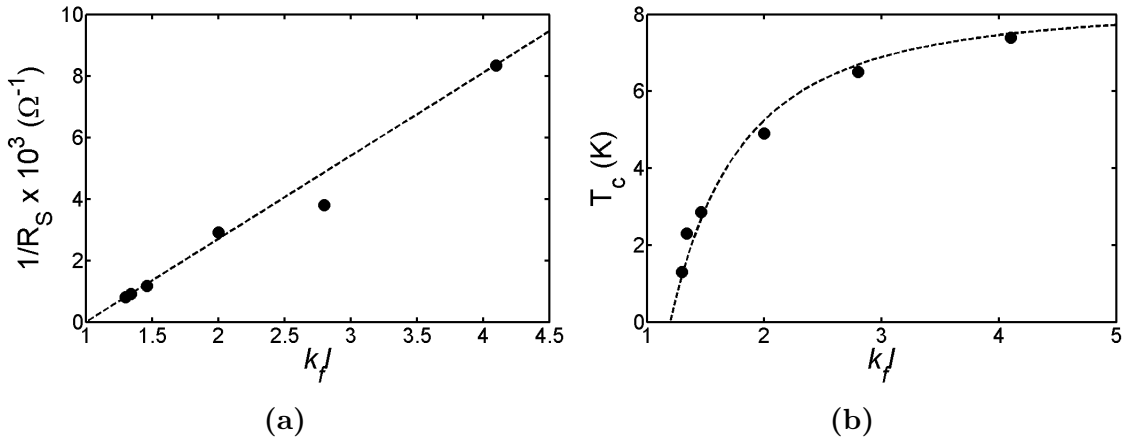


**Figure 13:** $k_f l$ dependence of a) sheet conductance (dots) with linear fit (dashed line), b) critical temperature (dots) fitted with Fiory-Hebard prediction (dashed line)

In order to explain the $k_f l$ dependence of the critical temperature, we used the relation introduced by Fiory and Hebard [72]:

$$\frac{T_c}{T_{c0}} = 1 - \frac{(k_f l)_c^2}{(k_f l)^2} : \tag{8}$$

From the fit, we obtained $T_{c0} = 8.2\ K$ and $(k_f l)_c = 1.2$, which is slightly larger than unity. From these results we can conclude, that the superconductivity is destroyed earlier than the insulating state is reached by increasing disorder in MoC. Therefore, the quantum phase transition from superconducting to insulating state has an intermediate metallic state as predicted by the fermionic scenario of SIT.

In the following section, we examine this scenario by analyzing further superconducting properties of our samples by means of a scanning tunneling microscope (STM).

## 0.3 Tunneling measurements

The transport measurement results presented in the previous section pointed out, that the superconductor - insulator phase transition has its intermediate metallic state. This scenario is called fermionic, because the Cooper pairs are first broken by increasing disorder to the conductive electrons, which are subsequently localized into the insulating state. The alternative scenario is bosonic, where the Cooper pairs survive with finite local $\Delta$, but they become localized. The ratio $2\Delta/k_BT_c$ increases in the bosonic scenario, as opposed to fermionic, where it keeps its constant value. Such behavior can be observed by measuring the density of states using a scanning tunneling microscope (STM).

We used STM for the measurement of samples with thickness 3, 5, 10 and 30 nm and the results are summarized in the paper [P7]. We showed that in MoC thin films $T_c$ and $\Delta$ decrease together with increasing disorder, which proves the fermionic scenario of SIT. Moreover, the scattering parameter $\Gamma$ , obtained by fitting the spectra with Dynes formula, is rapidly increasing as thickness decreases. Therefore, strong disorder leads to pair-breaking effects. Nevertheless, for thin films with $t \geq 5$ nm, long range phase coherence was confirmed by mapping of the Abrikosov vortex lattice. Presence of the vortex lattice means that there are no strong phase fluctuations, which become important for 3 nm thin films.

## 0.4 Field induced SIT in 3 nm MoC film

3 nm MoC thin films prepared on silicon (Si) and sapphire ($Al_2O_3$) substrate are close to SIT. As such, quantum phase transition to the normal state can also be achieved by increasing the external magnetic field above the upper critical field. We performed RT measurements at different values of applied magnetic field as well as the measurement of field dependence of the resistance at fixed temperatures. The results exhibited a rapid increase of the resistance for $T \to 0$ at $B > B_{c2}$. We showed, that in order to explain this behavior, the superconducting fluctuations combined with Altshuler-Aronov conductivity corrections should be taken into account.

Detailed measurements by STM under external magnetic field show, that the normal state reached by magnetic field has an atypical spectroscopic character in comparison with the normal state at $B = 0$ and $T > T_c$, where the constant density of states was measured. The deviation from the constant density of states is consistent with Altshuler-Aharonov logarithmic corrections caused by enhanced electron-electron interactions in disordered systems.

### Magnetotransport analysis

In Fig. 14, the RT characteristics at different values of fixed magnetic field are shown for both samples. The sheet resistance is normalized to the value $R_\square(50\ K) \approx 1100\Omega$. The relative deviation in highest magnetic field $B = 8$ T between the resistance measured at lowest temperature and at 20 K is very small $R(0.3\ \mathrm{K})/R(20\ \mathrm{K}) \approx 1.03$, which suggests that the field induced transition is fermionic, same as the thickness induced transition.

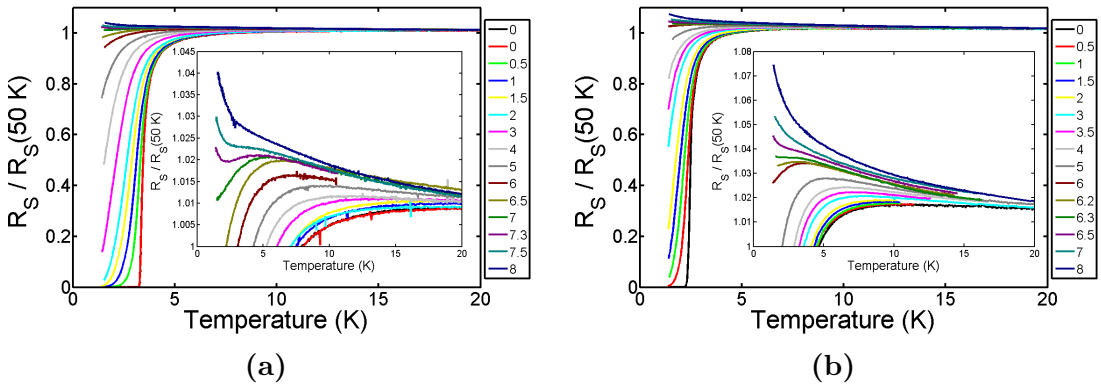


**Figure 14:** RT characteristics measured in magnetic field 0-8 T on 3 nm MoC sample depositend on a) silicon, b) sapphire substrate

From the results, temperature dependence of the upper critical field was determined (See Fig. 15) for different levels of superconducting transition. We can see, that the fields taken just before the resistance reaches zero qualitatively behave according to Werthamer-Helfand-Hohenberg prediction [67]. However, the fields taken at the beginning of the transition has almost the opposite character, which, in extrapolation, would give its divergence at limit $T \to 0$. Such atypical temperature dependence of $B_{c2}$ was discussed by Spivak in [73] as a consequence of mesoscopic fluctuations, when in mean field theory the superconducting solutions exist at arbitrary $B$.

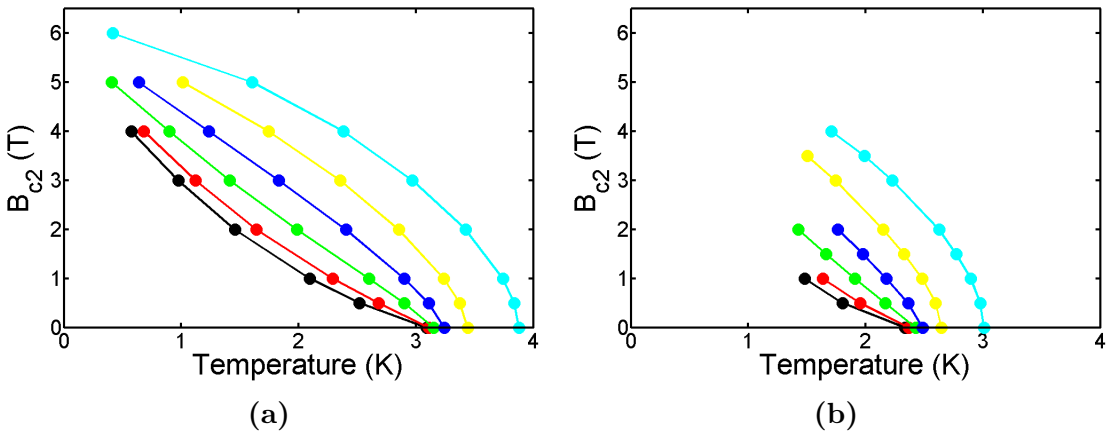


**Figure 15:** Extracted temperature dependence of upper critical field $B_{c2}$ taken at 95%, 75%, 50%, 25%, 10% and 5% level of superconducting transition for sample on a) silicon, b) sapphire substrate

In both graphs of RT characteristics in Fig. 14, we can see that for higher fields, the resistance starts to rapidly increase when $T \to 0$. Moreover, on the film deposited on silicon substrate, the strong reentrant can be seen before the resistance starts to increase. Such behavior can be explained by superconducting fluctuations in Cooper channel in 2D systems described by Galitzki and Larkin [74]. They analyzed three terms contributing to the conductivity: Aslamasov-Larkin (AL) term, which describes the conductivity of the fluctuating Cooper pairs; density of states (DOS), which decreases the conductance because of the lower number of electrons and the Maki-Thomson term, ascribed to the coherent scattering of normal electrons. They have shown, that all these three contributions have the same order, and they derived the final formula for the correction to conductivity:

$$\delta\sigma = \frac{4e^2}{3\pi h}\left[-\log\left(\frac{r}{b}\right) - \frac{3}{2r} + \Psi(r) + 4(r\Psi'(r) - 1)\right], \tag{9}$$

where $\Psi(x)$ is the logarithmic derivative of the $\Gamma$ function, $r = (1/2\gamma')(b/t)$ with $\gamma' = exp(\gamma) = 1.781$, and $t = T/T_{c0}$ and $b = (B - B_{c2}(T))/B_{c2}(0)$ are the reduced temperature and the reduced magnetic field.

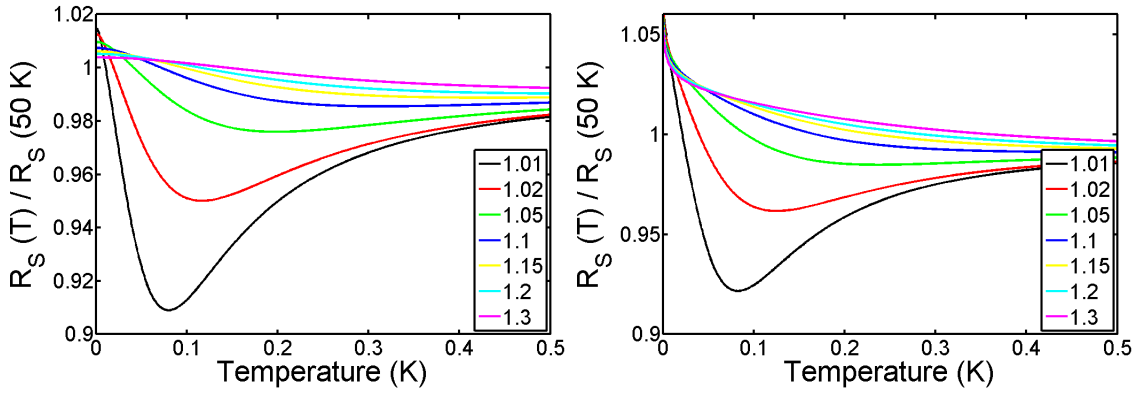


**Figure 16:** a) Galitzki-Larkin (GL) calculations of normalized resistance in different magnetic field $b = B/B_c$, b) GL + AA corrections

Fig. 16a shows the calculated curves for different values of magnetic field. We can see that the reentrant is observed, but in higher magnetic fields the resistance saturates. This is in contrast with our measurement, where the resistance exhibits a strong increase. As was discussed in detail by Gantmakher [35], the Althusler-Aronov term accounting for enhanced electron-electron interactions needs to be taken into account for highly disordered superconductors. Subsequently, the final relation takes the form:

$$R^{-1}(B,T) = \sigma_0 + \delta\sigma(B,T) - \alpha\frac{e^2}{h}\log\left(\frac{T}{T^*}\right), \tag{10}$$

where $\sigma_0$ is the classical conductivity, $\delta\sigma$ is the Galitzki-Larkin correction (Eq. 9) and the last term is the above mentioned Altshuler-Aronov correction with $T^*$ being the temperature at which this term diminishes. In Fig. 16b the calculated curves are shown. We can see, that the combination of GL and AA corrections to the conductivity provides the desired temperature dependence to resistance. Further improvement can be made by taking into account the atypical dependence of upper critical field $B_{c2}$, which could provide a far greater increase of the resistance and even better agreement with experiment. From the above, we can conclude that the normal state achieved by exceeding $B_{c2}$ much differs from the normal state for $T > T_c$. This behavior can be examined further by measuring the density of states by STM.

**STM analysis**

We have shown in Sec. **??** that the tunneling measurements provide information about the density of states, from which the superconducting energy gap $\Delta$ and scattering parameter $\Gamma$ can be determined. We performed the measurements at $B = 0$ and $T$=500 mK, on two samples deposited on silicon and sapphire substrate. The results were fitted by standard Dynes formula and they are shown in Fig. 17.

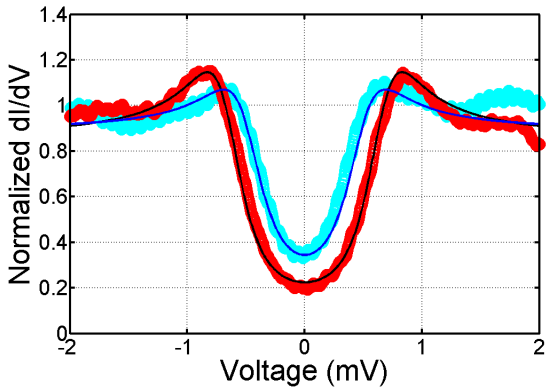


**Figure 17:** Comparison of tunneling differential conductance at $T \approx 500$ mK of 3 nm MoC film deposited on silicon (red) and sapphire (blue) substrate fitted with Dynes formula (solid lines). Obtained parameters were: $\Delta$ =0.66 meV, 0.49 meV; $2\Delta/kT_c$ =3.85, 3.85; $\Gamma$ =0.18 meV=0.27$\Delta$; 0.2 meV=0.41$\Delta$ for film on silicon and sapphire substrate respectively

The thin film deposited on silicon substrate has larger $\Delta$ and smaller scattering $\Gamma$ than the film on sapphire substrate. This is consistent with the RT characteristics, which exhibit superconducting transition at 3.97 K and 2.95 K for the silicon and sapphire substrates respectively. Since both samples have the same normal state sheet resistance $R_\square \approx 1100\Omega$ and the energy gap ratio $2\Delta/kT_c = 3.85$, we can assume that the substrate influences the superconducting properties, which are better for the Si substrate. The interface between the substrate and the film could lead to possible pair breaking, which is stronger for the sapphire substrate.

The topography by STM was made on both samples in order to examine the influence of the substrate on surface structure. The results displayed in Fig. 18 show the different structure of the samples.

While in the film on sapphire substrate the individual grains are well recognized, the film on silicon substrate has interesting boomerang-shaped structure. This could imply the different influence of the substrate on the epitaxial growth of the film.

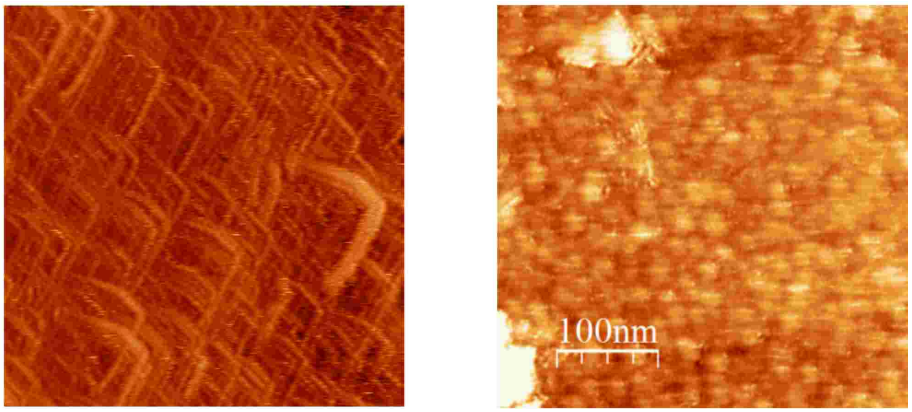


**Figure 18:** Surface topography taken by STM on 3 nm MoC film on a) silicon, b) sapphire substrate

Further experiments were performed on the MoC thin film on the silicon substrate. We measured the temperature dependence of the differential conductivity and the results are shown on graphs below (see Fig. 19).

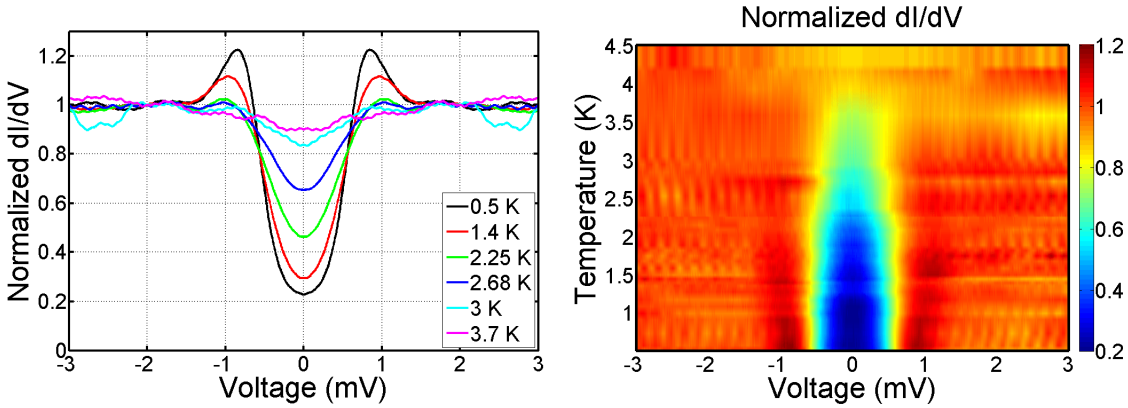


**Figure 19:** Temperature dependence of the normalized differential conductance of 3 nm MoC thin film on Si substrate measured by tunneling spectroscopy

On the 3D graphs we can see the decrease of the superconducting gap, which completely diminishes at $T_c \approx 4$ K. Above this temperature, the background is not changing anymore and it is approximately constant. Several differential conductance curves were fitted with the Dynes formula, from which we obtained the temperature dependence of $\Delta$ and $\Gamma$ (see Fig. 20). Closing of the superconducting gap with increasing temperature is in agreement with the BCS prediction. The scattering parameter $\Gamma$ increases with temperature, which was also found on thicker films presented in Sec. 0.3.

Since the differential conductance is normalized to its value at normal state, it can be assumed, that the superconducting features of the sample scale with the film surface, as opposed to the normal state features. We verified this assumption by

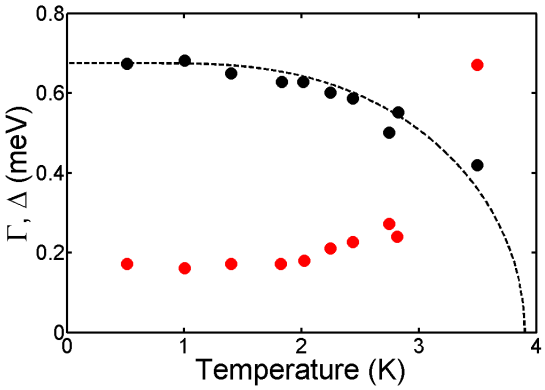


**Figure 20:** Temperature dependence of Dynes scattering parameter Γ (red dots) and the superconducting energy gap Δ (black dots) fitted with BCS theory (solid line)

comparing the Δ-map of the picked area of the sample with the topography image of the same area (See Fig. 21a,b).

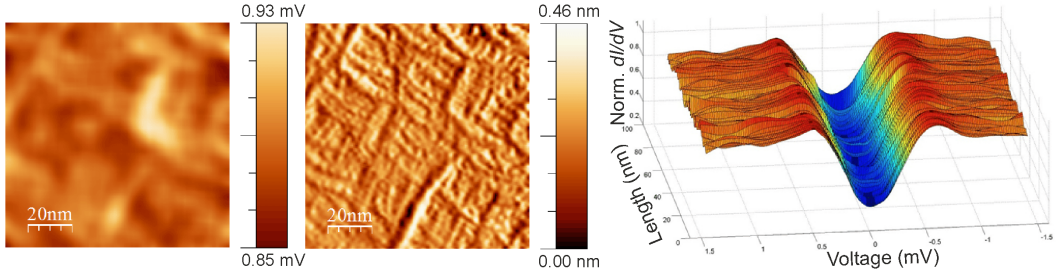


**Figure 21:** Comparison of a) Δ-map and b) surface topography taken by STM at the same area of 3 nm MoC film on silicon substrate. c) Differential conductance profile taken along 100 nm line

The relative fluctuations of Δ have the same order as the surface deviations. Fig. 21c shows that the fluctuations are sufficiently small to make a statement that the sample is superconducting homogeneous. Conductance mapping showed that the correlation between superconducting and surface properties completely diminishes when the voltage exceeds the superconducting energy gap. We can conclude that there are not remarkable superconducting features in the normal state.

### STM analysis under external magnetic field

Next, we focused on the density of states analysis by STM measurement of differential conductance under external magnetic field. As we mentioned earlier, the corrections to the conductivity caused by enhanced electron-electron interactions are characterized by Altshuler-Aronov (AA) effect [33], which has a logarithmic dependence in 2D disordered samples. For the density of states this correction has the following limits :

$$\delta N(E,T) \sim \begin{cases} \log(E\tau), & T \ll E \ll \tau^{-1} \\ \log(T\tau), & E \ll T \ll \tau^{-1} \end{cases} \tag{11}$$

In very large energy windows the logarithmic background saturates to the constant value $\log(T\tau)$ in limit $E \to 0$. We can assume the corrected density of states as follows:

$$N(E) = N_n + N_0 \left(1 + \log(E\tau)\right) \tag{12}$$

In STM we primarily measure the tunneling current in dependence on biased voltage. Taking the above formula 12, the analytic expression of the tunneling current and corresponding tunneling conductivity can be calculated:

$$\begin{aligned} I(V) &= C \int_{-\infty}^{\infty} N(E) \left[f(E) - f(E+V)\right] \\ I(V) &\overset{T\to 0}{=} CV \left(N_n + N_0 \log\left(\frac{V}{\tau}\right)\right) \\ \frac{I(V)}{V} &= C_1 + C_2 \log(V) \end{aligned} \tag{13}$$

This formula can be used to describe the experimental results obtained at $B$=8 T and $T$=0.4 K in appropriate limits (see Fig. 22).

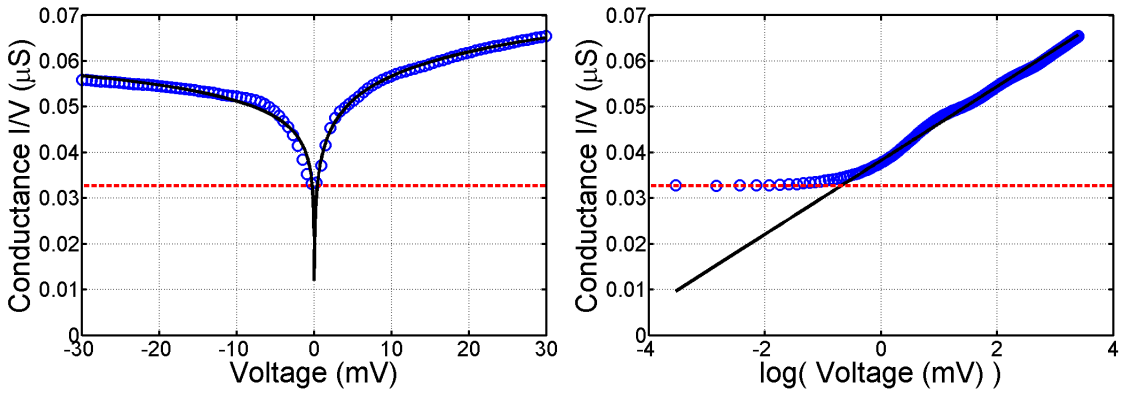


**Figure 22:** Tunneling conductance $I/V$ measured by STM (blue circles) at temperature $T \approx 400$ mK and magnetic field $B$ =8 T, fitted with the logarithmic voltage dependence (black solid line) for $E \gg T$ and the finite temperature saturation (red dashed line) for $T \gg E$. a) X-axis in linear scale from -30 mV to 30 mV, b) X-axis for logarithm of voltages from 0 to 30 mV

Logarithmic scale 22b shows that the background has the expected logarith-

mic dependence. The saturation at limit $E \to 0$ is much higher than it is expected from the ambient temperature (0.4 K). As such, we can introduce an effective temperature, that represents the scattering effect which increases the zero bias conductance. The value of this parameter can be determined spectroscopically from the intersection of two asymptotic curves (Eq. 11). The obtained values are in range 0.2 - 0.5 meV, which agrees with the Dynes parameter $\Gamma$ obtained at $B = 0$. One of the explanations could be a finite quasiparticle lifetime, which does not depend on external magnetic field. We will turn back to this concept later in microwave analysis of our samples (Sec. 0.6).

Small discrepancies from the logarithmic curve in Fig. 22 can be ascribed to the additional effects of the magnetic field. They should be more visible in spectroscopy of the differential conductance $dI/dV$ at low temperature, which directly reflects the density of states. Altshuler-Aronov effect in magnetic field at finite temperature leads to corrections in density of states (Eq. 6.1 in Ref. [75]):

$$\widetilde{\delta N}(E,T,B) = \widetilde{\lambda_0}\left\{ f\left(\frac{E}{T}\right) + \frac{\lambda_1}{2\lambda_0}\left[ f\left(\frac{E}{T}\right) + f\left(\frac{E+\omega_S}{T}\right) + f\left(\frac{E-\omega_S}{T}\right)\right]\right\}, \tag{14}$$

where $\omega_S = eB/m_e$ is cyclotron frequency and

$$f(x) = -\frac{1}{2}\int_0^{1/T\tau} dy \frac{1}{y}\frac{\sinh(y)}{\cosh(y)+\cosh(x)}$$

,

where $\tau$ is a relaxation time, which in our case satisfies the condition $\tau^{-1} \gg E$. The equation has 4 parameters $\tau^{-1}$, $T_{eff}$, $\widetilde{\lambda_0}$, $\frac{\lambda_1}{2\lambda_0}$, which have the following impact of the resulting DOS curve:

$\boldsymbol{\tau^{-1}}$: increases the curve by additive constant $\log(\tau^{-1})$. In our case, we fixed the value $\tau^{-1} = 0.1\ eV$, which is sufficiently high and in approximate agreement with results obtained by transport properties on similar samples (see Sec. 0.2).

$\boldsymbol{T_{eff}}$: smears the peak at $E \to 0$ and also the Zeeman splitting peaks at $E = \pm\omega_S$. It defines the value of the zero bias conductance.

$\widetilde{\boldsymbol{\lambda_0}}$: normalizes the whole curve.

$\frac{\lambda_1}{2\lambda_0}$:

- amplifies the logarithmic dependence as well as the deepening of the zero bias conductance with increasing magnetic field.
- we numerically found that in our case it should lie in interval $< -1/3\,, 0 >$.
- if $\frac{\lambda_1}{2\lambda_0} \to -1/3$: the deepening with increasing $B$ is strongest, but the logarithmic dependence at $B = 0$ vanishes.
- if $\frac{\lambda_1}{2\lambda_0} \to 0$: the logarithmic dependence at $B = 0$ is strongest, but the deepening with increasing $B$ vanishes (the Zeeman splitting peaks don't appear).
- if $\frac{\lambda_1}{2\lambda_0} < -1/3$ : the logarithmic dependence at B=0 changes its sign, which seems nonphysical.
- if $\frac{\lambda_1}{2\lambda_0} > 0$: peaks at $E = \pm\,\omega_S$ change their sign (deepening is changed to narrowing), which is opposite to our experiment, but such behavior was observed by Adams in [76]

We used the equation to fit the measured data of $dI/dV$ at $T$=640 mK and $B$=6 T$\approx B_{c2}$, where the superconducting DOS should not contribute. The results are shown in Fig. 23

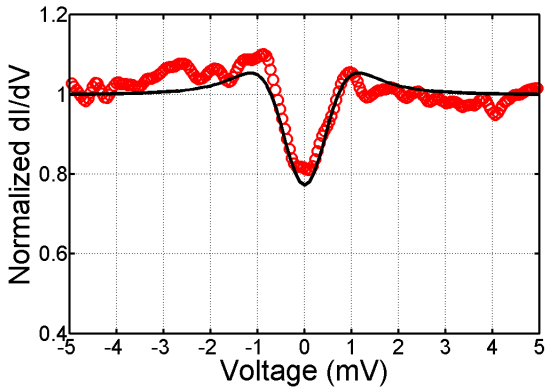


**Figure 23:** Normalized differential conductance measured by STM at temperature $T \approx 400$ mK and magnetic field $B = 6$ T (red circles) fitted with temperature dependent Altshuler-Aronov correction to DOS (black line)

The obtained effective temperature is $T_{eff} = 3.4\ K = 0.3\ meV$, which agrees with values obtained spectroscopically with approximate limit equations. The deviations of measured data are caused by larger noise in high magnetic field amplified by numerical differentiation of the measured $I(V)$ curves.

In order to fit the experimental data at finite magnetic fields below $B_{c2}$ we have to combine the AA contribution with the superconducting DOS as follows:

$$N(E) = N_S(E)(1 + \delta N(E)), \tag{15}$$

where $N_S$ is defined by Dynes formula:

$$N_S(E) = \frac{E + i\Gamma}{(E + i\Gamma)^2 - \Delta(B,T)^2}, \tag{16}$$

where $\Delta(B,T)$ can be approximately obtained from following relations:

$$\begin{aligned} \frac{\Delta(T)}{\Delta(0)} &= \tanh\left(\frac{\Delta(T)}{\Delta(0)}\frac{T_C}{T}\right) \\ \frac{\Delta(B)}{\Delta(0)} &= \sqrt{1 - \left(\frac{B}{B_{C2}}\right)^2}. \end{aligned} \tag{17}$$

In Fig. 24 the calculated curves for superconducting DOS, AA correction and their combination respectively in magnetic fields from 0 T to 8 T are shown.

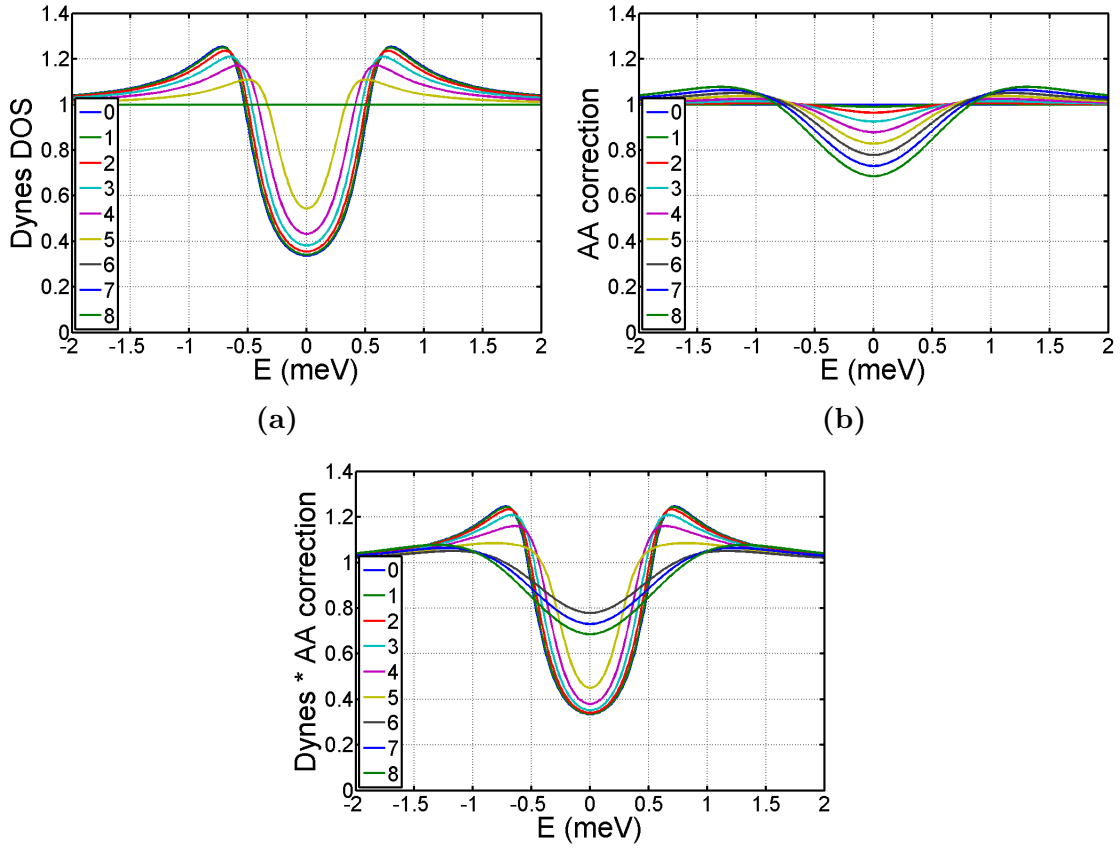


**Figure 24:** Simulated curves of DOS in magnetic fields from 0 to 8 T according to a) Dynes formula, b) Altshuler-Aronov (AA) correction, c) combination of Dynes and AA

Finally, we can compare the measured data with the theoretical curves in the whole range of magnetic fields displayed on 3D graphs (see Fig. 25).

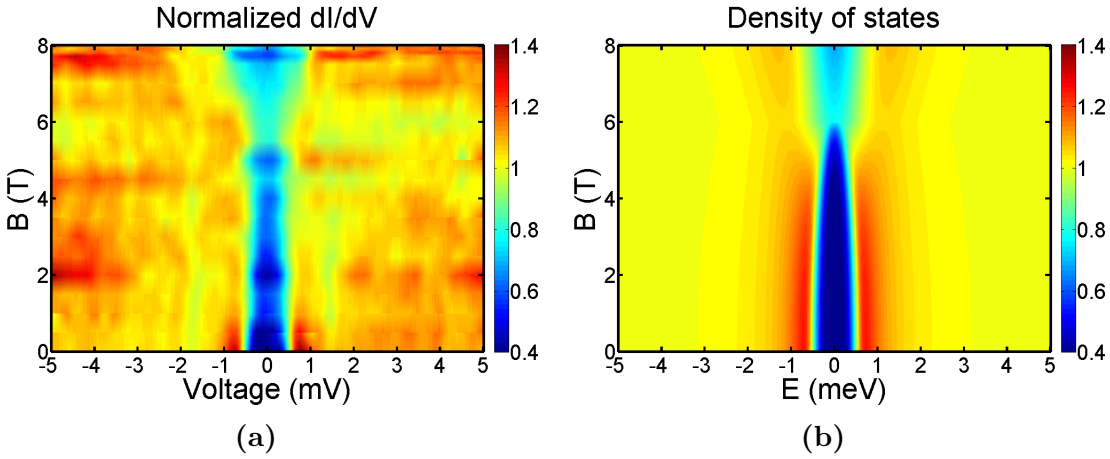


**Figure 25:** 3D plot of the magnetic field dependence of a) normalized differential conductance measured by STM, b) DOS simulated by combination of superconducting and AA contributions

We can see that the curves, calculated from Eq. 14 using Dynes formula, describe the measured data very well. The results qualitatively agree for a wide

range of magnetic fields. The energy gap is closing with increasing magnetic field, with the minimum in upper critical field $B_{c2}$, above which it is opening again because of other, non-superconducting effects. This effect could be ascribed to Zeeman splitting in paramagnetic limit, which has the same order as the superconducting energy gap ($\sim$1 meV). The deepening of the zero bias conductance with magnetic field above $B_{c2}$ can also corresponds to a rapid increase of sheet resistance observed by transport measurements.

We can conclude that the normal state achieved by magnetic field has peculiar character and considerably differs from the normal state in $B = 0$ at temperatures exceeding the critical temperature $T_c$. In both cases, the deviations can be ascribed to AA effects in a disordered system.

## 0.5 Nanobridge in MoC thin film

The optimized 10 nm MoC thin films were patterned with nanobridges by electron lithography at IPHT Jena, Germany. Four-probe transport measurements were performed in cryogenic assembly in our laboratory. The results are summarized in the paper [P5].

## 0.6 Microwave analysis

Complex conductivity characterizes the microwave response of a superconductor. Its real and imaginary parts represent the contribution of the normal electrons and Cooper pairs, respectively. The dependence on external electromagnetic field is well described by Mattis-Bardeen theory, introduced in theoretical review (see Sec. **??**). The complex conductivity can be directly measured, using a coplanar waveguide (CPW) resonator patterned on the superconducting thin films. As it is shown in section **??**, the quality factor of a CPW resonator reflects the dissipative losses in the material, so $Q \sim 1/\sigma_1$, while the resonant frequency represents the inductive reflections caused by the kinetic inductance of Cooper pairs (besides the geometrical factors), so $\omega_0 \sim \sigma_2$.

Disorder in superconductors directly affects CPW resonator behavior. In this section, we present a microwave analysis of homogeneously disordered MoC thin films and show that scattering effects are significantly stronger than it is expected by original MB theory. Subsequently we analyze a granular $MgB_2$ thin film, where scattering is weak, but the tunneling between individual granules causes detuning of the resonant frequency in magnetic field, which is characteristic of RF-SQUID structures.

### 0.6.1 MoC CPW resonator

We prepared and measured several samples of MoC thin films (see Tab. 3) on which a CPW resonator was patterned by optical lithography and dry ion-etching. The resonator was designed to have a quality factor $Q_{ext} = 30\ 000$ and a resonant frequency $\omega_0 = 2\pi \times 2.5$ GHz for films with a high thickness, where scattering is negligible ($Q_{int} \gg Q_{ext}$). This was verified on the 200 nm thick MoC film (sample 4). If the thickness is lowered close to or even below superconducting coherence length, the kinetic inductance is increased, which decreases the resonant frequency. Moreover, the scattering process driven by interface scattering centers considerably suppresses the internal quality factor. Films with 10 nm thickness are optimal for further implementation of quantum nanostructures [10], so a more detailed examination of their behaviour in microwave electromagnetic field is needed.

| | $\mathbf{R_{\square}(\Omega)}$ | **t(nm)** | $\mathbf{T_c(K)}$ | **Q** | $\mathbf{f_0(GHz)}$ |
|---|---|---|---|---|---|
| Sample 1 | 173 | 10 | 5.8 | 9600 | 1.42 |
| Sample 2 | 182 | 10 | 7.2 | 24000 | 1.51 |
| Sample 3 | 169 | 10 | 5.5 | 8300 | 1.35 |
| Sample 4 | 18 | 200 | 6.7 | 30000 | 2.49 |
| Sample 5 | 380 | 5 | 3.8 | 1700 | 0.75 |

**Table 3:** Summarized properties of the MoC CPW resonator samples

We measured the temperature dependence of the resonant frequency and the loaded quality factor of our samples. The measured curves were compared with the Mattis-Bardeen theory **??**. The obtained complex conductivity was then recalculated to complex impedance by using *FastHenry 3.0* software, with input values $\sigma_1$ and $\lambda = \sqrt{1/\mu\omega\sigma_2}$ and output of the form of $Z = R + i\omega L$. From the real and imaginary impedance, we can directly determine $Q$ and $\omega_0$ by using the well known relations [38].

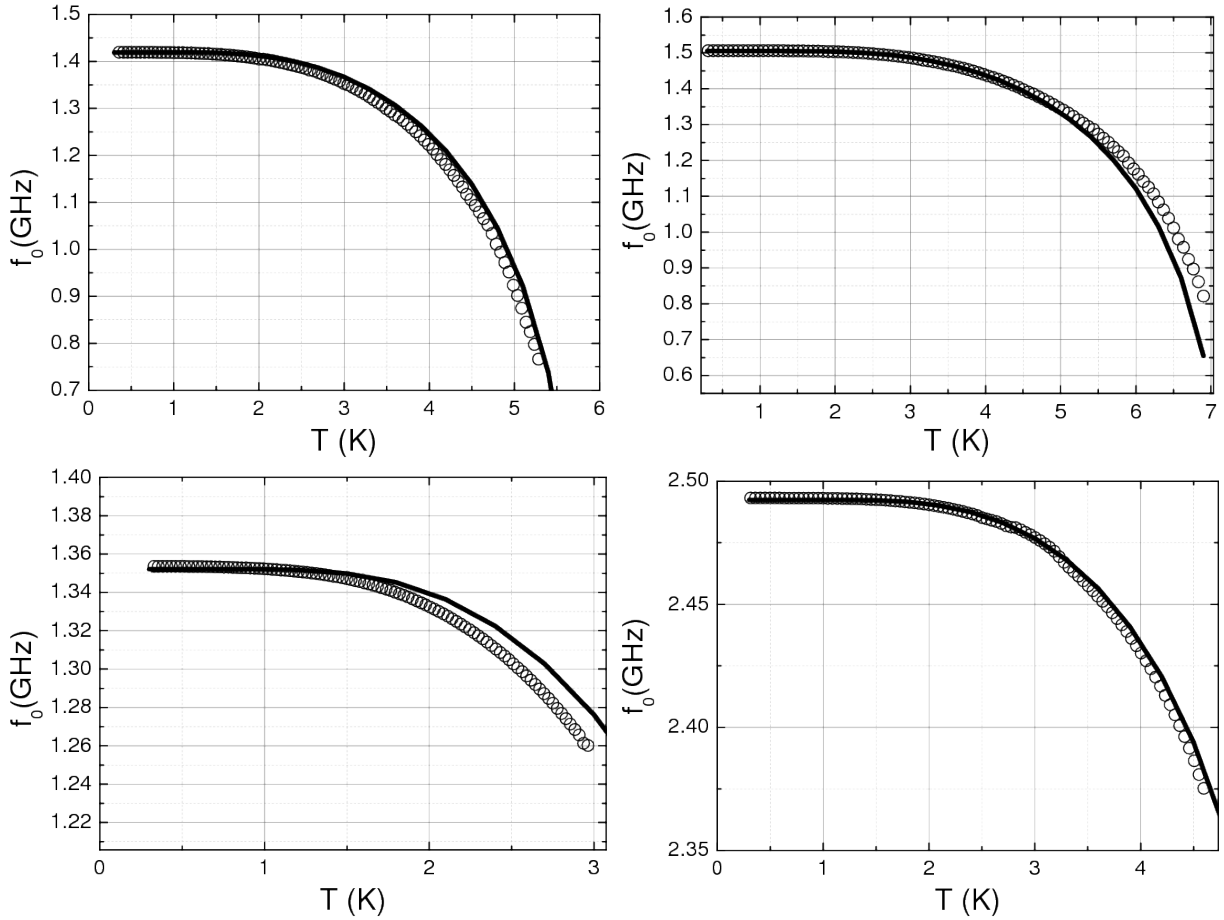


**Figure 26:** Temperature dependence of the resonant frequency (circles - measured data, lines - theoretical model) for samples 1, 2, 3, 4 respectively

In Fig. 26, we compare the measured data of the resonant frequency for samples 1-4 with the numerical model and as we can see, the theoretical curves fit the measured data very well.

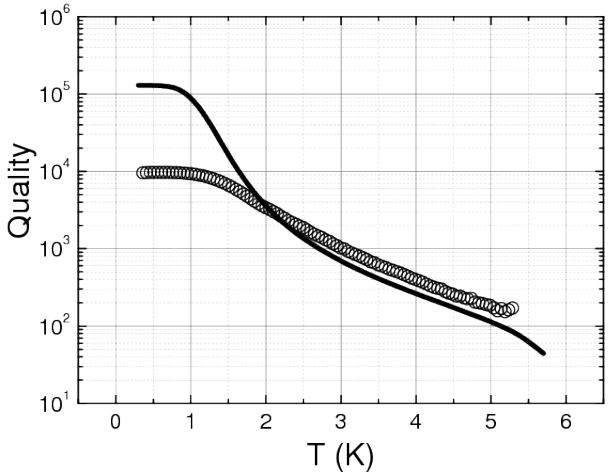


**Figure 27:** Temperature dependence of the quality factor (circles - measured data, lines - theoretical model) for 10 nm MoC sample

The same model was used to describe the quality factor temperature dependence. The internal quality factor was calculated from attenuation constant, which is defined by the real part of the impedance **??**. From the results (Fig. 27) we can see, that the difference is considerable in a wide temperature range. The standard MB model is therefore not appropriate to describe the dissipative losses in the disordered superconductors, because of the enhanced scattering effects. A modification of the model was made by the introduction of the finite quasiparticle lifetime. The modified model fits our data very well. The details are presented in the paper [P6].

As it has been mentioned above, the modified Mattis-Bardeen model is applicable in wide frequency range, so it can be used in order to fit the experimental data from THz spectroscopy. We performed such measurements at Institute of Physics, Academy of Sciences of the Czech Republic, Prague on the 20 nm MoC film. The results fitted with the model are presented in Fig. 28. The temperature of the experiment was too high ($T = 0.8\ T_c$) to resolve, if there is a peculiarity at $\omega = \Delta$.

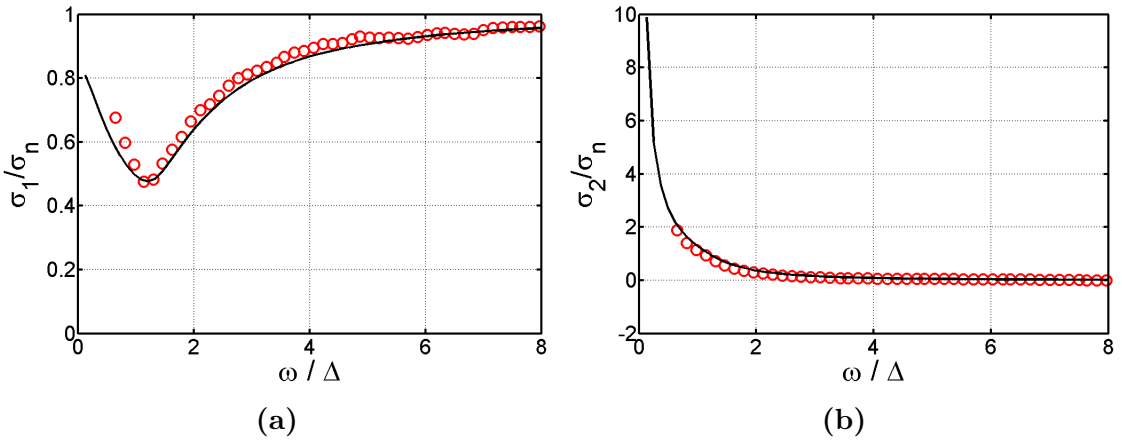


**Figure 28:** Terahertz spectroscopy measurement of the real part (a) and the imaginary part (b) of the complex conductivity (red circles) fitted with modified Mattis-Bardeen model (solid line) for parameters: $T = 0.8\ T_c$, $\Delta = 1.24$ meV and $s = 0.25$ meV=0.2 $\Delta$

However, the experimental results obtained in MoGe and NbN superconductors demonstrated in Ref. [77,78], exhibited the peculiarity even at higher temperatures. One of the explanation can be provided by the concept of the nonequlibrium processes [14], which could be present in the THz experiments due to the large power of the THz pulses. Such processes lead to redistribution of the quasiparticles, which causes the effective cooling of the sample. As it was discussed by Scalapino [79], this effect is strongest in region $(\Delta/2, 2\Delta)$, which is qualitatively consistent with the mentioned experimental results and also with the Nam model at low temperatures.

One of our future plans in this field is to perform additional THz measurements on several samples with different properties and analyze them with deeper theoretical concept considering the mentioned processes.

### 0.6.2 $MgB_2$ CPW resonator

The same technique of the CPW resonator and MB model was also used in granular $MgB_2$ thin film with thickness 300 nm. The temperature dependence of the complex conductivity is well described by standard Mattis-Bardeen formulas, from which we can conclude that the scattering in this material is much lower than in homogeneously disordered superconductors. In addition, we measured the dependence of the resonant frequency at the lowest temperature in our microwave cryogenic assembly ($\sim$300 mK). Surprisingly, hysteretic periodic detuning was observed. Such behaviour is characteristic of artificially patterned RF-SQUID, where the detuning is caused by Josephson inductance, which depends on external magnetic field (see Sec. **??**). We proposed the model of percolation path interrupted by the naturally created insulating barrier between grains. The more detailed view of the model as well as the measurement results are shown in paper [P1].

# 1 Conclusions

In the submitted thesis, we focused on the analysis of thin films of highly disordered superconductors. The preparation of MoC thin films by magnetron sputtering was tuned in order to obtain optimal sample properties. The results were samples with maximized critical temperature $T_c$ and enhanced sheet resistance $R_\square$. Material properties, such as structure, stoichiometry and surface roughness were analyzed by means of XRD, EDX and STM. The resulting thin films are superconductive homogeneous and have cubic $\delta$-phase crystallographic structure of MoC with decreased carbon content due to lattice vacancies.

Magneto-transport and Hall effect measurements determined that the critical temperature $T_c$ is well correlated with sheet resistance $R_\square$ and Ioffe-Regel disorder parameter $k_f l$, rather than with film thickness. We showed that Finkelsten's formula can not be applied in order to explain the $T_c$ suppression, despite the fact that it qualitatively well describes the transport properties of the disordered superconducting thin films.

The results from tunneling spectroscopy demonstrated an increase of in-gap states with decreasing thickness. Moreover, a vortex lattice was observed, proving the long range phase coherence ascribed to the fermionic scenario of superconductor-insulator transition (SIT).

A more detailed view of the field induced SIT of 3 nm MoC thin film revealed an atypical normal state as opposed to the normal state achieved by temperature. Results of magneto-transport and STM measurements were in agreement with the Altshuler-Aronov model of enhanced electron-electron interactions. The superconducting properties of the same MoC samples prepared on different substrates (Si and $\mathrm{Al}-2\mathrm{O}_3$) were somewhat different, proving that the interface between the substrate and the thin film plays a role as a possible pair breaker.

Homogeneous superconducting properties of our thin films near SIT predestine them for nanotechnology applications. Such prospects were outlined by the transport measurements of a nanobridge patterned on 10 nm MoC film, which exhibited quantum phase slip-like behavior.

Scattering effects were also analyzed by microwave measurement of CPW res-

onators patterned in 10 nm and 5 nm MoC films. In order to describe the decrease of internal quality factor and resonance frequency, a modification of Mattis-Bardeen theory for complex conductivity was made. Finite quasiparticle lifetime as a possible source of scattering was introduced as a fitting parameter, and the results agreed with the Dynes phenomenological parameter $\Gamma$ obtained from STM. The new model is applicable in a wide frequency range, which was proved by a terahertz spectroscopy measurements of $\sigma_1$ and $\sigma_2$.

The same CPW technique was used for a granular $MgB_2$ superconductor. The results showed periodic hysteretic detuning in magnetic field, which is characteristic of artificially prepared RF SQUID nanostructures. A reasonable model of percolation path interrupted by weak links between the grains was designed and successfully applied in the fit.

Future plans in the research include further detailed examination of the interface between superconducting thin film and substrate, and transport measurements in higher magnetic fields which could provide an even better understanding of superconductor-insulator transition in our samples. Since the technology of sample deposition is optimized and provides reproducible results, application in nanowires with enhanced kinetic inductance is planned as well. A new design will be proposed and the quantum properties will be examined in dilution $^3$He-$^4$He refrigerator. Finally, the knowledge acquired from MoC investigation will be used in preparation and application of other disordered superconductors such as WSi, $W_3Si_5$, NbN, TiN, etc.

# Bibliography

[1] J. B. Pendry. Negative refraction makes a perfect lens, Phys. Rev. Lett. 85 (2000) 3966.

[2] W. Cai, U.K. Chettiar, A.V. Kildishev, and V.M. Shalaev, Optical cloaking with metamaterials, Nature Photon. 1, 224 (2008).

[3] A. L. Rakhmanov, A. M. Zagoskin, Sergey Savel'ev, and Franco Nori., Quantum metamaterials: Electromagnetic waves in a Josephson qubit line, Phys. Rev. B 77, 144507 (2008).

[4] M. Grajcar et al., Nature Physics, 4 (2008) 612.

[5] E. Il'ichev, Y. S. Greenberg, Europhys. Lett. 77 (2007) 58005.

[6] A. A. Houck et al., Nature 449 (2007) 328.

[7] O. Astafiev et al., Nature 449 (2007) 588.

[8] M. Wegener et al., Toy model for plasmonic metamaterial resonances coupled to two-level system gain, OPTICS EXPRESS 16 (2008) 19785.

[9] G. Romero, J. J. Garcia-Ripoll and E. Solano, Microwave Photon Detector in Circuit QED, arXiv:0811.3909v1.

[10] O. V. Astafiev, Coherent quantum phase slip, Nature 484 (2012) 355–358.

[11] W. Escoffier, C. Chapelier, N. Hadacek, and J.-C. Villegier, Phys. Rev. Lett. 93, 217005 (2004).

[12] V. M. Vinokur, T. I. Baturina, M. V. Fistul, A. Y. Mironov, M. R. Baklanov, and C. Strunk, Nature 452, 613 (2008).

[13] A. D. Zaikin, D. S. Golubev, A. van Otterlo, and G. T. Zimanyi, Phys. Rev. Lett. 78, 1552 (1997).

[14] M. Tinkham, Introduction to Superconductivity: Second Edition (McGraw-Hill, Inc., 1996).

[15] E. Il'ichev, V. Kuznetsov, and V. Tulin, JETP Lett. 56, 295 (1992).

[16] J. E. Mooij and Y. V. Nazarov, Nat Phys 2, 169 (2006).

[17] T. I. Baturina, D. Kalok, A. Bilui, V. M. Vinokur, M. R. Baklanov, A. K. Gutakovskii, A. V. Latyshev, and C. Strunk, Appl. Phys. Lett. 102, 042601 (2013).

[18] T. I. Baturina, D. Kalok, A. Bilui, V. M. Vinokur, M. R. Baklanov, A. K. Gutakovskii, A. V. Latyshev, and C. Strunk, Appl. Phys. Lett. 102, 042601 (2013).

[19] A. M. Goldman, Int. J. Mod. Phys. 24, 4081 (2010).

[20] E. F. C. Driessen, P. C. J. J. Coumou, R. R. Tromp, P. J. de Visser, and T. M. Klapwijk, Phys. Rev. Lett. 109, 107003 (2012).

[21] P. C. J. J. Coumou, E. F. C. Driessen, J. Bueno, C. Chapelier, and T. M. Klapwijk, Phys. Rev. B 88, 180505 (2013).

[22] A. F. Ioffe a A. R. Regel, Non-crystalline, amorphous and liquid electronic semiconductors, Prog. Semicond. 4, 237 (1960)

[23] J. Bardeen, L. N. Cooper and J. R. Schrieffer, Phys. Rev.106, 162(1957).

[24] D. Mattis, J. Bardeen, Theory of the anomalous skin effect in normal and superconducting metals, PHYSICAL REVIEW 111 (1958) 412.

[25] LONDON F. and LONDON H. The electromagnetic Equations of the Supraconductor. Proc. Roy. Soc.(London) A149, 71 (1935)

[26] V. L. Ginzburg and L. D. Landau, Zh. Eksp. Ter. Fiz. 20, 1064 (1950)

[27] I. Giaever, Electron Tunneling Between Two Superconductors, Phys Rev Lett 5, 147, 464 (1960).

[28] M. Mahel a kol: Supravodivosť; MFFUK 1997

[29] JOSEPHSON, B. D. 1962. Possible new effects in superconductive tunnelling. Phys. Lett. 1, 251 (1962)

[30] Ilichev, Wagner, Fritzsch, Kunert, Schultze, , May, Hoenig, Meyer, Graj-car, Born, Krech, Fistul, Zagoskin, Characterization of superconducting structures designed for qubit realizations, Applied Physics Letters 80 (2002).

[31] N. D. Ashcroft a N. D. Mermin, Solid State Physics, Brooks & Cole, 1976.

[32] P. W. Anderson, Absence of Diffusion in Certain Random Lattices, Phys. Rev. 109, 1492 (1958).

[33] B. L. Altshuler a A. G. Aronov, Electron-electron Interactions in Disordered Systems, Elsevier, (1985).

[34] S. J. Lee and J. B. Ketterson, Phys. Rev. Lett. 64, 3078 (1990).

[35] V. F. Gantmakher a V. T. Dolgopolov, Superconductor-insulator quantum phase transistion, Phys. Usp. 53, 1 (2010).

[36] A. I. Larkin, Superconductor-insulator transitions in films and bulk materials, Ann. Phys. (Leipzig) 8, 785 (1999).

[37] D. M. Pozar, Microwave Engineering (Addison-Wesley Publishing Company, 1993).

[38] M. Göppl, A. Fragner, M. Baur, R. Bianchetti, S. Filipp, J. M. Fink, P. J. Leek, G. Puebla, L. Steffen, and A.Wallraff: Coplanar Waveguide Resonators for Circuit Quantum Electrodynamics; arXiv:0807.4094v1 [cond-mat.supr-con]

[39] SIMONS, R. N. 2001: Coplanar Waveguide Circuits, Components, and Systems; ISBN 0-471-22475-8

[40] K. Watanabe, K. Yoshida, T. Aoki and S. Kohjiro: Kinetic Inductance of Superconducting Coplanar Waveguides; Jpn. J. Appl. Vol. 33 (1994) pp. 5708-5712

[41] J. E. Mooij and C. J. P. M. Harmans: New Journal of Physics; New Journal of Physics7(2005) 219, doi:10.1088/1367-2630/7/1/219

[42] R. E. Collin, Foundations for Microwave Engineering, 2nd ed., New York: McGraw-Hill, 1992, pp. 178—179.

[43] M. Žemlička, Meranie a numerická analýza supravodivých koplanárnych rezonátorov, FMFI UK, diplomová práca (Bratislava 2012)

[44] G. Ventura and L. Risegari,The Art of Cryogenics, Elsevier (2008), ISBN: 978-0-08-044479-6.

[45] http://cryomech.com/

[46] http://www.oxford-instruments.com/products/cryogenic-environments/3heinserts/cryogen-free-helium-3-refrigerators/cryogen-free-helium-3-refrigerator-helioxacv?src=mn

[47] http://www.keycom.co.jp/eproducts/upj/top.htm

[48] T. P. Devereaux and D. Belitz, Phys. Rev. B 44, 4587 (1991).

[49] R. C. Dynes, J. P. Garno, G. B. Hertel, and T. P. Orlando, Phys. Rev. Lett. 53, 2437 (1984).

[50] A. Bruno, G. de Lange, S. Asaad, K. L. van der Enden, N. K. Langford, and L. DiCarlo, Appl. Phys. Lett. 106, 182601 (2015).

[51] A. Plecenik, M. Grajcar,S. Benacka, P. Seidel, and A. Pfuch, Phys. Rev. B 49, 10016 (1994).

[52] S. B. Nam, Phys. Rev. 156, 470 (1967).

[53] D. Sherman, U. S. Pracht, B. Gorshunov, S. Poran, J. Jesudasan, M. Chand, P. Raychaudhuri, M. Swanson, N. Trivedi, A. Auerbach, M. Scheffler, A. Frydman, and M. Dressel, Nat Phys 11, 188 (2015).

[54] D. Sherman, B. Gorshunov, S. Poran, N. Trivedi, E. Far-ber, M. Dressel, and A. Frydman, Phys. Rev. B 89, 035149 (2014).

[55] M. Swanson, Y. L. Loh, M. Randeria, and N. Trivedi, Phys. Rev. X 4, 021007 (2014).

[56] K. Likharev, Dynamics of josephson Junctions and Circuits, CRC Press, 1986.

[57] Ilichev, Wagner, Fritzsch, Kunert, Schultze, , May, Hoenig, Meyer, Graj-car, Born, Krech, Fistul, Zagoskin, Characterization of superconducting structures designed for qubit realizations, Applied Physics Letters 80 (2002).

[58] M. Gregor, T. Plecenik, R. Sobota, J. Brndiarova, T. Roch, L. Satrapinskyy, P. Kus, A. Plecenik, Influence of annealing atmosphere on structural and superconducting properties of MgB2thin films, Appl. Surf. Sci. (2014).

[59] Gupta, Sen, Shashawati, Singh, Aswal, Khare, Neeraj, Direct evidence of weak-link grain boundaries in a polycrystalline mgb2 super-conductor, Journal of Applied Physics 97 (2005).

[60] P. Macha, S. H. W. van der Ploeg, G. Oelsner, E. Ilichev, H.-G. Meyer, S. Wunsch, and M. Siegel, Appl. Phys. Lett. 96, 062503 (2010).

[61] A. M. Finkelshtein, JETP Lett 45, 46 (1987).

[62] A. M. Finkelshtein, Phys B 197, 636 (1994).

[63] J. Simonin, Surface term in the superconductive Ginzburg-Landau free energy: Application to thin films, Phys. Rev. B 33, 7830 (1986)

[64] M. Žemlička, Microwave and tunneling measurements of superconductors, rigorous thesis, FMFI UK, Bratislava (2015)

[65] M. Žemlička, Preparation and Measurement of Ultra-thin Superconducting Films, written part of the dissertation exam, FMFI UK, Bratislava (2014)

[66] A Theoretical Treatise on the Electronic Structure of Designer Hard Materials, dissertation, Uppsala (2001)

[67] N. R. Werthamer, E. Helfand, and P. C. Hohenberg, Temperature and Purity Dependence of the Superconducting Critical Field, Hc2. III. Electron Spin and Spin-Orbit Effects, Phys. Rev. 147, 295 (1966)

[68] J. M. Graybeal and M. R. Beasley, Phys. Rev. B 29, 4167 (1984)

[69] B. Sacépé, C. Chapelier, T. I. Baturina, V. M. Vinokur, M. R. Baklanov, and M. Sanquer, Phys. Rev. Lett. 101, 157006 (2008).

[70] T. I. Baturina and V. M. Vinokur, Ann. Phys. 331, 236 (2013).

[71] S. V. Postolova, A. Yu. Mironov, M. R. Baklanov, V. M. Vinokur, and T. I. Baturina, poster at International workshop on strongly disordered superconductors and the superconductor-insulator transition, Villard de Lans, 2014, unpublished.

[72] T. Fiory and A. F. Hebard, Phys. Rev. Lett. 52, 2057 (1984).

[73] B. Spivak and Fei Zhou, Mesoscopic Effects in Disordered Superconductors near Hc2, Phys. Rev. Lett. 74, 2800 (1995).

[74] V. M. Galitski and A. I. Larkin, Phys. Rev. B 63, 174506 (2000)

[75] Efros, Pollak, Electron-electron interactions in disordered systems, Modern Problems in Condensed Matter Science, Vol. 10 (1985).

[76] Adams, Spin Effects Near the Superconductor-Insulator Transition, Louisiana State University, LA 70803.

[77] M. Šindler, R. Tesař, J. Koláček, L. Skrbek, and Z. Šimša, Far-infrared transmission of a superconducting NbN film, Phys. Rev. B 81, 184529 (2010).

[78] H. Tashiro, Unusual thickness dependence of the superconducting transition of $\alpha$-MoGe thin films, Phys. Rev. B 78, 014509 (2008).

[79] Jhy-Jiun Chang and D. J. Scalapino, Nonequilibrium Superconductivity, Journal of Low Temperature Physics, 31 (1978).

[80] G. J. Milburn, Phys. Rev. Lett. 62, 2124 (1989).

[81] J. Bourassa, J. M. Gambetta, A. A. Abdumalikov Jr, O. Astafiev, Y. Nakamura, A. Blais, Phys. Rev. A 80, 032109 (2009).

[82] E. A. Tholén, A. Ergul, K. Stannigel, C. Hutter, arXiv:0906.2744v2 (15 Nov 2009).

# List of publications and conferences

**Publications:**

[P1] M. Žemlička, P. Neilinger, M. Trgala, M. Grajcar, M. Gregor, T. Plecenik, P. Ďurina: Superconducting properties of magnesium diboride Thin Film Measured By Using Coplanar Waveguide Resonator, **Applied Surface Science**, 312, 231–234 (2014)

[P2] M. Trgala, M. Žemlička, P. Neilinger, M. Rehák, M. Leporis, S. Gaži, J. Greguš, T. Plecenik, T. Roch, E. Dobročka, M. Grajcar: Superconducting MoC thin films with enhanced sheet resistance, **Applied Surface Science**, 312, 216–219 (2014)

[P3] P. Neilinger, M. Rehák, M. Gregor, M. Žemlička, T. Pleceník, M. Trgala, P. Ďurina, M. Grajcar: Periodic response of superconducting high quality MgB2 resonator to magnetic field, APCOM Proceedings 2013

[P4] M. Žemlička, D. Manca, P. Neilinger, M. Grajcar: Cryogenic carbon powder filters for superconducting qubit measurement, Proceedings of ADEPT 2014

[P5] M. Žemlička, P. Neillinger, M. Rehák, M. Trgala, D. Manca, U. Hübner, E. Ilichev, M. Grajcar: Transport properties of nanobridges created on molybdenum carbide superconducting films, APCOM Proceedings 2014

[P6] M. Žemlička, P. Neilinger, M. Trgala, M. Rehák, D. Manca, M. Grajcar, P. Szabo, P. Samuely, Š. Gaži, U. Hübner, V. M. Vinokur, E. Ilichev: Finite quasiparticle lifetime in disordered superconductors, **Physical Review B** 92, 224506 (2015)

[P7] P. Szabó, T. Samuely, V. Hašková, J. Kačmarčík, M. Žemlička, M. Grajcar, J. G. Rodrigo, P. Samuely: Fermionic scenario for the destruction of superconductivity in ultrathin MoC films evidenced by STM measurements, **Physical Review B** 93, 014505

**Conferences:**

[C1] *Canadian Quantum Information Students' Conference 2013*, 24-28 June 2013, Institute for Quantum Science and Technology, University of Calgary, Canada. Poster: Finite quasiparticle lifetime as possible source of decoherence in superconducting circuits

[C2] *20th conference of Slovak physicists*, 2-9 September 2013, Bratislava, Slovakia. Poster: Microwave measurement and analysis of disordered superconductors with finite quasiparticle lifetime

[C3] *Solid State Surfaces and Interfaces*, 24-28 November 2013, Smolenice, Slovakia. Poster: Superconducting properties of magnesium Diboride Thin Film Measured By Using Coplanar Waveguide Resonator

[C4] *Physics and applications of superconducting hybrid nano-engineered devices*, 31 August - 4 September 2014, Santa Maria Castellabate, Italy. Poster: Finite quasiparticle lifetime in the surface layer of disordered superconductors.

[C5] *Week of Doctoral Students 2015 focused on physical study branches*, 2–4 June 2015, Prague, Czech republic. Lecture: Finite quasiparticle lifetime in disordered superconductors.